buildings

MDPI

Article

Effects of Different Inhibitors on the Corrosion Mitigation of Steel Rebar Immersed in NaCl-Contaminated Concrete Pore Solution

Sang-Ho Min [1], Han-Seung Lee [1,*] and Jitendra Kumar Singh [2,3]

[1] Department of Architectural Engineering, Hanyang University ERICA, 55 Hanyangdaehak-ro, Sangrok-gu, Gyeonggi-do, Ansan-si 15588, Republic of Korea; tkdghals@daum.net
[2] Innovative Durable Building and Infrastructure Research Center, Center for Creative Convergence Education, Hanyang University (ERICA Campus), 1271 Sa-3-dong, Sangnok-gu, Ansan 15588, Republic of Korea; jk200386@hanyang.ac.kr
[3] Department of Chemistry, Graphic Era Deemed to be University, Bell Road, Clement Town, Dehradun, Uttarakhand 248002, India
* Correspondence: ercleehs@hanyang.ac.kr

Abstract: The corrosion of steel rebar embedded in concrete under marine conditions is a major global concern. Therefore, it needs a proper corrosion mitigation method. Various types of corrosion inhibitors are used to mitigate the corrosion of steel rebar in chloride-contaminated concrete; however, selecting the appropriate inhibitor and determining its optimal concentration remains a concern. Therefore, in the present study, three types of inhibitors—calcium nitrite (CN: $Ca(NO_2)_2$), N,N′-dimethyl ethanol amine (DMEA: $(CH_3)_2NCH_2CH_2OH$), and L-arginine (LA: $C_6H_{14}N_4O_2$) in three different concentrations, i.e., 0.3, 0.6 and 1.2 M—were compared with a control (without inhibitor, i.e., blank) sample to determine the optimum concentration of the inhibitor for corrosion resistance performance evaluation of reinforcement bars immersed in 0.3 M NaCl-contaminated concrete pore (NCCP) solution for various durations. The corrosion resistance properties were assessed using open circuit potential (OCP), electrochemical impedance spectroscopy (EIS) with immersion duration, and potentiodynamic polarization (PDP) after 168 h of exposure. The results showed that the CN inhibitor performed exceptionally well (corrosion inhibition efficiency greater than 97%) in terms of corrosion resistance. However, due to its hazardous nature and its ban in the U.S. and European Union, CN cannot be used in construction. In comparison, while DMEA showed some effectiveness, LA performed better and is also eco-friendly. The corrosion resistance efficiency of samples containing 0.6 M LA remains above 97% even after 168 h of immersion in the NCCP solution. This efficiency is consistent throughout the entire immersion period, from 1 h to 168 h. Therefore, it is recommended that LA be used as a corrosion inhibitor for steel reinforcement bars instead of CN, particularly in chloride-contaminated concrete, as it is both effective and safer than CN.

Keywords: steel; corrosion; inhibitor; open circuit potential (OCP); electrochemical impedance spectroscopy (EIS); potentiodynamic polarization (PDP)

Citation: Min, S.-H.; Lee, H.-S.; Singh, J.K. Effects of Different Inhibitors on the Corrosion Mitigation of Steel Rebar Immersed in NaCl-Contaminated Concrete Pore Solution. *Buildings* **2024**, *14*, 3559. https://doi.org/10.3390/buildings14113559

Academic Editor: Grzegorz Ludwik Golewski

Received: 21 October 2024
Revised: 1 November 2024
Accepted: 6 November 2024
Published: 7 November 2024

1. Introduction

Studying the corrosion mechanisms of steel rebar, inhibitors, and coating/paint systems in diverse environmental conditions is crucial for understanding their long-term behavior. Corrosion, an electrochemical process resulting from the interaction between steel and its environment, is influenced by factors such as humidity, salinity, acidity, and the presence of pollutants. These factors significantly accelerate corrosion, particularly in harsh environments like marine, industrial, or highly acidic areas. Corrosion not only leads to substantial maintenance and replacement costs, especially in infrastructure exposed to aggressive conditions, but it also compromises the structural integrity of bridges, buildings,

pipelines, and industrial machinery. Understanding and controlling corrosion before failure occurs is essential for safety and economic reasons. By studying corrosion mechanisms, risks can be mitigated through appropriate design, material selection, and the application of protective measures.

The corrosion of steel structures is an imperative issue worldwide. Therefore, various corrosion mitigation methods, such as use of stainless steel, hot-dip galvanizing (HDG), epoxy coating, and inhibitors, have been used for steel rebar [1]. Stainless steel rebar is very expensive and causes pitting corrosion in chloride-contaminated concrete conditions. HDG is galvanically active and amphoteric, leading to accelerated corrosion in the alkaline environments of concrete and forms corrosion products. These corrosion products cause internal pressure within the concrete, potentially resulting in structural failures [2–5]. Achieving a defect-free epoxy coating on steel rebar is challenging, and studies have shown that polymeric coatings like epoxy reduce bonding with concrete due to differences in thermal expansion. Once corrosion initiates beneath the coating, it becomes difficult to control [6]. Therefore, using corrosion inhibitors is recommended over these protective approaches.

The use of corrosion inhibitors is cost effective and easy to apply through simple mixing, which has drawn increasing attention from researchers and engineers for their application to reduce steel corrosion [7–9]. Corrosion inhibitors are used to reduce the rate of corrosion in aggressive concrete environments. The application of a corrosion inhibitor is one of the best mitigation processes to reduce the corrosion of embedded steel rebar in concrete [10,11]. There are many types of inorganic, organic, and hybrid inhibitors being used worldwide. Based on their performance, they are also classified as anodic, cathodic, and mixed types of inhibitor. The salts of silicate, phosphate, molybdate, zinc, cerium, nitrate, and nitrite are inorganic-based inhibitors and these are widely used [12].

Nitrite-based inhibitors, especially calcium nitrite, are most effective and used to control the corrosion of steel rebar [13]. Moreover, calcium nitrite inhibitors require an insignificant amount to obtain maximum corrosion resistance performance, otherwise it causes adverse effect such as developing cracks in the concrete [14–17]. However, it is not recommended to use by European Union and U.S.A. due to their toxic and harmful effect on human beings [18]. Therefore, the other inorganic inhibitors, i.e., phosphate-based inhibitors, are being recommended by researchers to use in concrete [19–21]. The phosphate ions transform the unstable iron oxide/hydroxides into stable ones and delay the onset of the corrosion [22,23].

The organic corrosion inhibitors are mostly amine and alcohol with long carbon chains, which effectively adsorbed onto the steel rebar and form a passive film, thereby reducing the corrosion reaction. Inorganic inhibitors and various heteroatoms that are present donate lone pairs of electrons to the iron surface. This interaction allows the molecules to adsorb onto the surface, effectively reducing the corrosion reaction [24]. The tetrabutylammonium bromide (TBAB) reduces the corrosion of steel rebar in concrete by forming a film and adsorption phenomenon, which acts as barrier and restricts the ingress of Cl^- ions and oxygen [15,25]. The amine-based inhibitor was better than the traditional nitrite-based inhibitor in the concrete environment owing to the formation of the protective passive film [26,27]. Therefore, it is said that the amine-based inhibitor, i.e., mono-, di-, and triethanol- amine performed well in a chloride-containing concrete environment by forming passive layer [28–30]. The amino-based corrosion inhibitor generally acts as the migratory inhibitor where it diffuses and adsorbs onto the steel rebar surface and reduces the further corrosion [24,31,32].

There is a scarcity in the literature comparing the corrosion resistance properties of organic- and inorganic-based inhibitors in NaCl-contaminated concrete conditions to accurately assess corrosion kinetics of the inhibitor, and so it is essential to study the passivation behavior and pitting tendencies. Therefore, in the present study, the corrosion resistance properties of different concentrations of calcium nitrite (CN), dimethyl ethanol amine (DMEA), and L-arginine (LA) were chosen to understand the corrosion kinetics and

mechanisms by various electrochemical experiments, such as open circuit potential (OCP), electrochemical impedance spectroscopy (EIS), and potentiodynamic polarization (PDP). These techniques provide valuable insights into the corrosion kinetics and mechanisms of steel rebar in a 0.3 M NaCl-contaminated concrete pore (NCCP) solution at different durations of immersion. And lastly, the morphology of the surface film formed in the NCCP solution after 168 h of immersion was studied by the scanning electron microscopy (SEM) and chemical composition by energy-dispersive spectroscopy (EDS).

2. Materials and Methods

To determine the corrosion resistance of different inhibitors, a 16 mm diameter steel rebar was cut from 1000 mm length into 10 mm height. The cross section of steel rebar was abraded from 60 to 1200 grit size emery paper followed by cloth polish with fine alumina (0.5 μm particle size) slurry using an automated polishing machine to obtain a defect-/scratch-free surface. The chemistry of the steel rebar as shown in Table 1 was used in the present study for the corrosion studies. Prior to use, the polished steel rebar was degreased with acetone to remove the contaminants that came after polishing.

Table 1. Elemental composition of steel rebar used in the present study.

Elements (wt.%)										
C	**Si**	**Mn**	**P**	**S**	**Ni**	**Cr**	**Cu**	**Mo**	**Sn**	**Fe**
0.235	0.250	0.90	0.014	0.006	0.028	0.037	0.018	0.009	0.002	98.501

The different types of inhibitors, i.e., calcium nitrite (Sigma Aldrich, Seoul, South Korea), L-arginine (Sigma Aldrich, Seoul, South Korea), and N,N′-dimethylethanolamine (Daejung Chemicals, Seoul, South Korea) were chosen for the corrosion resistance properties determination. The analytical grade of KOH, NaOH, CaO, and NaCl were purchased from Daejung Chemicals, Seoul, South Korea for the synthesis of the NaCl-contaminated concrete pore (NCCP) solution, i.e., control sample. These chemicals have been used without further purification. The NCCP solution was prepared by dissolving 0.208 M NaOH, 0.06 M KOH, 0.035 M CaO, and 0.3 M NaCl in distilled water [21,33,34]. The solution was stirred on automatic magnetic stirrer (MS300HS, MTOPS, Seoul, Korea) at 500 RPM until 24 h, thereafter; the solution was filtered out by 5C number (110 mm) Wattman paper to remove the insoluble CaO. The inhibitors, i.e., calcium nitrite (CN), dimethylethanolamine (DMEA), and L-arginine (LA) were mixed and dissolved in the NCCP solution and the detailed concentration of the inhibitors are shown in Table 2. The solution has a pH in the range of 12 to 13, indicating it is strongly alkaline.

Table 2. Concentration of inhibitors in NCCP solution.

Inhibitor	Concentration of Inhibitor (M)	pH of the Solution
Control (NCCP solution)	0	13.00
Calcium nitrite (CN)	0.3	12.13
	0.6	11.94
	1.2	11.76
Dimethyl ethanol amine (DMEA)	0.3	13.03
	0.6	13.07
	1.2	13.19
L-arginine (LA)	0.3	12.96
	0.6	12.91
	1.2	12.84

The corrosion resistance performance of the control and various inhibitors was evaluated in NCCP solution, using a working area of 0.78 cm^2. Electrochemical impedance spectroscopy (EIS) was conducted with a Potentiostat (VersaSTAT, Princeton Applied Research, Oak Ridge, TN, USA) applying a 10 mV sinusoidal voltage across a frequency range from 100 kHz to 10 mHz at the open circuit potential (OCP) of the sample.

Potentiodynamic polarization (PDP) tests were performed on the samples after 168 h of immersion. The tests were carried out from −0.4 V to +0.8 V versus a saturated calomel electrode (SCE) at a scan rate of 0.166 mV/s. All corrosion performance assessments were conducted in triplicate, and the average results are reported in the manuscript. The electrochemical data analysis was performed using NOVA 1.10 software.

The surface morphology and chemical composition of the film formed on the steel rebar after 168 h of immersion in NCCP (control) and 0.6 M LA containing solutions was characterized using field emission-scanning electron microscopy (FE-SEM, MIRA3, TESCAN, Brno, Czech Republic) at 15 kV equipped with energy-dispersive spectroscopy (EDS).

3. Results and Discussion

3.1. Electrochemical Measurements

3.1.1. OCP Determination

The open circuit potential (OCP) of steel rebar immersed in different inhibitors is illustrated in Figure 1. From Figure 1a, it is clear that the control sample (without inhibitor), i.e., the NCCP solution, exhibits a more active OCP compared to the samples containing varying concentrations of CN. This is attributed to localized or pitting corrosion caused by Cl^- ions [35]. As immersion time increases, the OCP of both the control and the sample with a low CN concentration (0.3 M) shifts in the active direction, again, due to the effect of Cl^- ions in the solution. For the control sample, the OCP stabilizes after 96 h of immersion, likely due to the deposition of oxides or corrosion products on the steel surface, continuing through 168 h of immersion [36]. However, the low CN concentration (0.3 M) is insufficient to sustain the formation of a stable oxide or passive film, leading to the breakdown of the film by Cl^- ions and initiating corrosion [37]. In contrast, as the CN concentration increases, the OCP shifts towards a more positive direction over the immersion period, indicating the formation of a protective oxide or passive film on the steel rebar, which enhances corrosion resistance. An interesting observation is noted with the DMEA inhibitor, where increasing the concentration of DMEA results in the OCP shifting towards a more active direction over time, as shown in Figure 1b. This suggests that higher amounts of DMEA disrupt the passive film, initiating the corrosion process by dissolving the metal without forming a protective corrosion layer. This behavior aligns with previous studies, which have shown that amino-alcohol-based inhibitors like DMEA can cause corrosion in certain conditions by failing to maintain a stable protective layer [38,39]. Despite this, the steel rebar with DMEA, even at higher concentrations, still exhibits a nobler OCP compared to the control sample. This indicates that DMEA does provide some degree of corrosion protection in chloride-contaminated environments, although its effectiveness may diminish with increasing concentration. It is important to note that for steel samples containing LA, different concentrations of the inhibitor display varying levels of corrosion protection. As shown in Figure 1c, concentrations of LA either higher or lower than 0.6 M exhibit a more active OCP. However, all LA concentrations result in a nobler OCP compared to the control sample, which is attributed to the adsorption of LA molecules and the formation of a passive film on the steel surface. The authors explained that a specific concentration of LA, acting as a zwitterion, interacts with a fixed amount of Cl^- ions to form a zwitterion-(Cl)-Fe complex, which provides corrosion protection [40,41]. In the present study, the OCP results suggest that 0.6 M LA, in combination with 0.3 M NaCl, offers the optimal balance to neutralize all Cl^- ions. When the LA concentration is either lower or higher than this optimal amount, the zwitterion interacts directly with the Fe instead of the Cl^- ions. In this scenario, Cl^- ions first bind to the Fe, followed by the zwitterion, forming a zwitterion-(Cl)-Fe complex [42]. If the LA concentration is lower than NaCl, the Cl^- ions

promote the breakdown of the passive film. On the other hand, at higher LA concentrations, the negative end of the zwitterion interacts with Fe to form a zwitterion-Fe complex, which is unstable and offers less corrosion protection. It is noteworthy that, initially, all samples, including the control, CN, and LA (except 0.6 M), showed signs of corrosion initiation, as their OCP values are lower than −0.270 V vs. SCE. This threshold is commonly used to indicate corrosion initiation, as described in previous studies [43,44]. As observed in Figure 1a, the CN inhibitors at concentrations of 0.6 M and 1.2 M shifted the OCP towards the passive direction, suggesting the formation of a protective film on the steel rebar, which helps prevent corrosion. In contrast, the DMEA inhibitor, despite shifting the OCP in a positive direction as shown in Figure 1b, remained within the corrosion initiation category. In the case of LA, Figure 1c shows that the 0.6 M concentration exhibited a passive potential, which is attributed to the formation of the zwitterion-(Cl)-Fe complex. This complex likely consumes all Cl^- ions present in the solution, effectively preventing further corrosion.

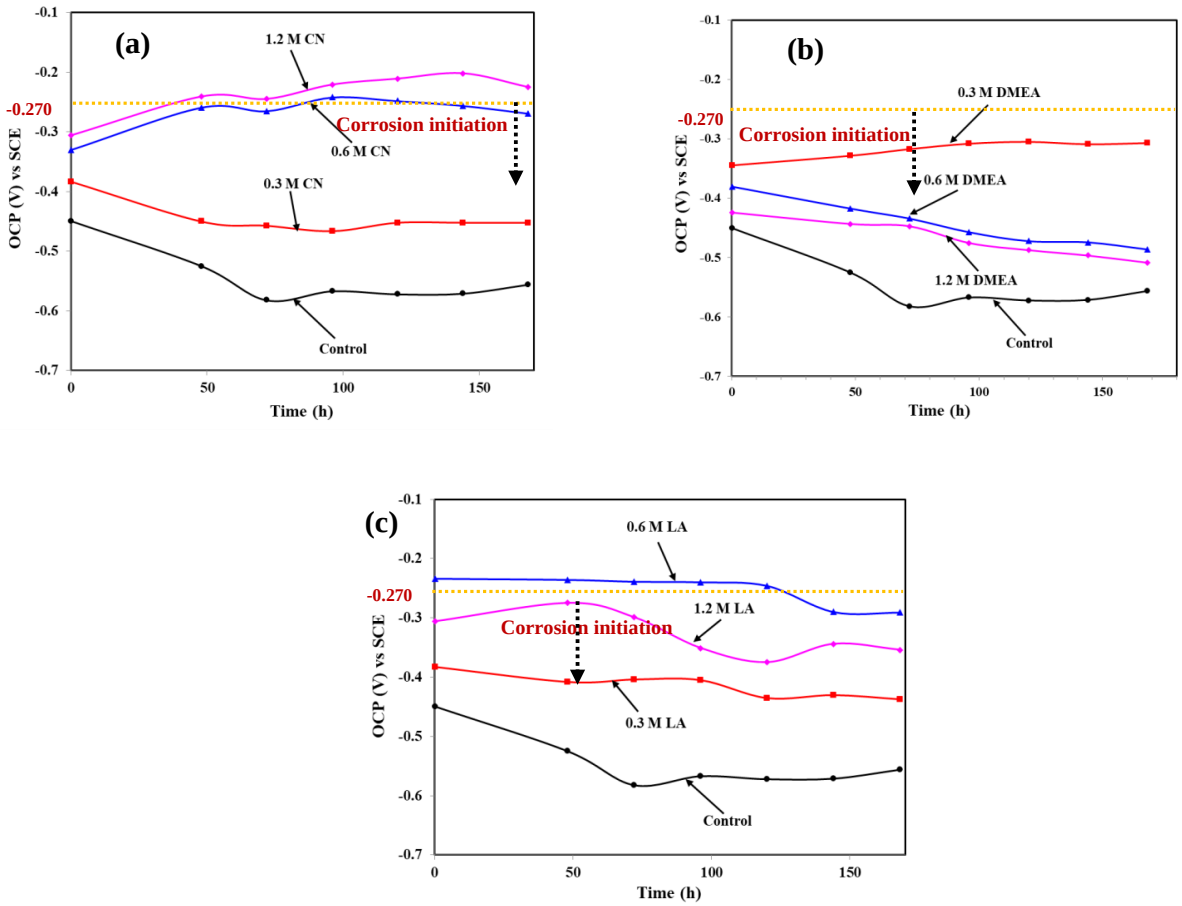

Figure 1. The OCP measurements of steel rebar immersed in NCCP solutions containing different concentrations of (**a**) CN, (**b**) DMEA, and (**c**) LA inhibitors across various immersion periods.

3.1.2. EIS Studies

The electrochemical impedance spectroscopy (EIS) results after 1 and 168 h of immersion for the samples are shown in Figures 2–5. Figure 2 displays the Nyquist plots following 1 h of immersion, comparing samples with three inhibitors—CN, DMEA, and LA—against a control sample without any inhibitors. As observed in Figure 2a–c, the control sample shows the smallest magnitude, a result of the breakdown of the passive film by Cl^- ions in the alkaline solution. In contrast, samples immersed in CN inhibitors demonstrated increased Nyquist plot magnitudes, proportional to the amount of CN used. This increase is attributed to the oxidation of iron into stable iron oxides, which form a passive layer, blocking the active corrosion sites on the steel surface [45,46]. Furthermore,

the Nyquist plots for CN inhibitors show a higher magnitude at lower frequencies than at higher frequencies, indicating that the corrosion process is mainly controlled by charge transfer resistance (R_{ct}) at low frequencies. This suggests that ion transfer from the steel surface (Fe) is restricted by the passive film, with the film becoming more protective at higher concentrations of CN, as shown by the larger low-frequency capacitive loop.

When steel rebar is immersed in a DMEA-containing solution, the Nyquist plot magnitude is lower than that of the CN but greater than the control sample as shown in Figure 2b. At higher DMEA concentrations, the protective film on the steel surface becoming destabilized is attributed to the formation of a carbonate film, where the adsorption of methyl and ethyl groups from DMEA is more pronounced than the nitrogen atom's interaction with the steel and the mean time, the Cl^- ions induces the corrosion reaction. According to Welle et al. (1997), this reduces the interaction of the nitrogen atom's lone pair of electrons with iron (Fe), which diminishes the adsorption of the inhibitor molecules onto the steel surface [47]. As a result, DMEA-containing samples exhibit smaller Nyquist plot dimensions compared to the CN sample. Figure 2b shows that at high concentrations of DMEA, the Nyquist plot at high frequency (inset of Figure 2b) has a very small dimension, indicating film destabilization. However, the low-frequency Nyquist plot dimension for the 0.3 M DMEA sample is greater (inset of Figure 2b), indicating the formation of a stabilized protective film due to the adsorption of the inhibitor molecules.

The corrosion resistance properties of the LA-containing sample after 1 h of immersion are shown in Figure 2c. From this figure, it is evident that the Nyquist plot dimensions of the LA sample are larger than those of the DMEA sample but smaller than those of the CN sample. However, the CN inhibitor is not suitable for construction due to its hazardous nature, and it has been banned by both the European Union and the U.S.A. Therefore, LA emerges as the most effective inhibitor, providing superior performance and being eco-friendly, making it suitable for use in construction. The concentration of LA is crucial, as concentrations either higher or lower than 0.6 M result in reduced Nyquist plot dimensions. At 0.3 M LA, there is a low amount of zwitterion present, and the Cl^- content (0.3 M NaCl) exceeds the ability of the zwitterion to combine with both Cl^- and Fe to form the zwitterion-(Cl)-Fe complex. On the other hand, at 1.2 M LA, the zwitterion ions are more abundant than the Cl^- ions in the solution. As a result, the negative pole/end of the zwitterion interacts directly with positive Fe (Fe^{++}) rather than with Cl^-, forming a zwitterion-Fe complex that is less protective than the zwitterion-(Cl)-Fe complex. This can be observed from the low-frequency Nyquist plot, where the plot size is larger compared to the dimensions at low and middle frequencies, indicating a charge transfer resistance (R_{ct}) resulting in high corrosion resistance.

The Bode plots of the samples after 1 h of exposure are presented in Figure 3. As shown in Figure 3a, increasing the concentration of CN results in a rise in the total impedance of the sample at the lowest studied frequency, i.e., 0.01 Hz, which is attributed to a greater degree of Fe oxidation into a stable oxide film that impedes the attack of Cl^- ions. The phase angle Bode plot for the CN inhibitor reveals two time constants at mid and low frequencies. The mid-frequency capacitive loop corresponds to the formation of a passive film caused by the CN inhibitor, while the low frequency is associated with the charge transfer resistance (R_{ct}). As the inhibitor concentration increases, the phase angle maxima at mid frequency shift to higher values, reaching $-80°$, indicating that the oxide/passive film becomes more protective and homogeneous. Additionally, the broadening of the phase angle at both mid and low frequencies suggests robust film formation with capacitive behavior. Thus, at higher CN inhibitor concentrations, the total impedance is at its maximum.

In the case of DMEA, the lowest studied concentration performs exceptionally well in terms of total impedance at 0.01 Hz compared to higher concentrations, as shown in Figure 3b. This performance is attributed to the adsorption of inhibitor molecules, where the nitrogen atom in the amine group donates a lone pair of electrons to the vacant d-orbital of Fe, forming a electrostatic/covalent bond [48]. However, at higher concentrations, the methyl and ethyl groups of DMEA interact with Fe and destabilize the bond between

nitrogen and Fe [47]. As the concentration of the inhibitor increases, the total impedance at 0.01 Hz gradually decreases. Nevertheless, DMEA-containing samples still show higher total impedance compared to the control sample (Figure 3b). The phase frequency Bode plots for DMEA inhibitor-containing samples are also depicted in Figure 3b. The orientation and shape of the phase angle for both the control and 1.2 M DMEA samples are quite similar, showing a phase angle maximum of around −70° at middle frequencies, which suggests the formation of an oxide film. However, at lower frequencies, the phase angle maximum reduces to around −10°, indicating the formation of a porous and unstable oxide film. On the other hand, the 0.3 M DMEA sample exhibits a phase angle maximum of approximately −40° at low frequencies, indicating the presence of an adherent and protective adsorbed film, primarily due to the charge transfer resistance (R_{ct}).

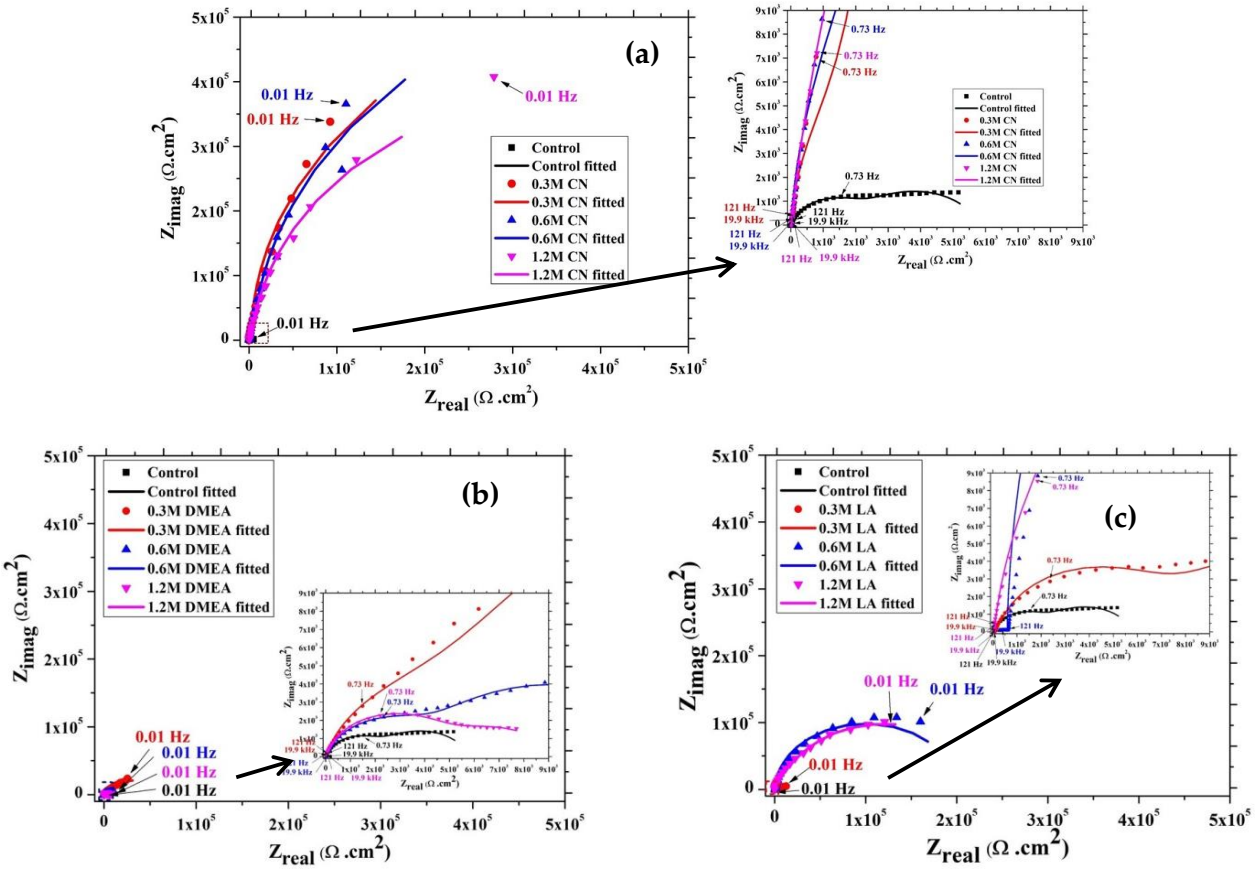

Figure 2. The Nyquist plots of steel rebar immersed in NCCP solution with different concentrations of (**a**) CN, (**b**) DMEA, and (**c**) LA after 1 h.

The total impedance of LA-containing inhibitors after 1 h of immersion in NCCP solution is illustrated in Figure 3c. The LA-containing samples exhibit higher impedance values compared to the control, attributed to the adsorption of inhibitor molecules and the formation of a complex on the steel rebar surface. The sample containing 0.6 M LA displayed the highest total impedance at 0.01 Hz, which is linked to the formation of a stable and protective zwitterion-(Cl)-Fe complex film on the steel rebar. However, in the case of lower and higher than 0.6 M LA, the total impedance is lower attributed to the significant amount of Cl^- ions in solution, which perturb the film and formation of zwitterion-Fe complex rather than zwitterion-(Cl)-Fe complex, respectively. Moreover, from 0.3 M to 0.6 M LA, the impedance is gradually increased, but once the concentration is greater than 0.6 M LA, it is decreased owing to the adsorption of zwitterion through the carboxylic, i.e., negative end of LA; therefore, there is the weak bonding between –COO and Fe in the zwitterion-Fe complex [40–42]. Furthermore, from 0.3 M to 0.6 M LA, the

impedance gradually increases, but beyond 0.6 M LA, it decreases. This is attributed to the adsorption of the zwitterion through the carboxylic (negative) end of LA, resulting in a weak bond between $–COO^{-}$ and Fe^{++} in the zwitterion-Fe complex. The phase angle Bode plots, shown in Figure 3b, reveal that the samples exhibit distinct characteristics with two time constants at middle and low frequencies. The phase angle maximum for the 0.3 M LA sample shifts towards lower frequencies compared to the control, indicating film formation, although its phase angle is lower than that of the 0.6 M and 1.2 M LA samples at mid frequency. For the 0.6 M LA sample, the phase angle maximum shifts towards a lower frequency, around −80°, suggesting that corrosion is predominantly controlled by film formation, where the charge transfer resistance (R_{ct}) is very high. This implies that the film is homogeneous and compact, as supported by SEM results (discussed in the passive film characterization section). Additionally, the broadening of the phase angle maximum for the 1.2 M LA sample at mid frequency, also around −80°, indicates that the adsorbed film is protective and exhibits capacitive properties.

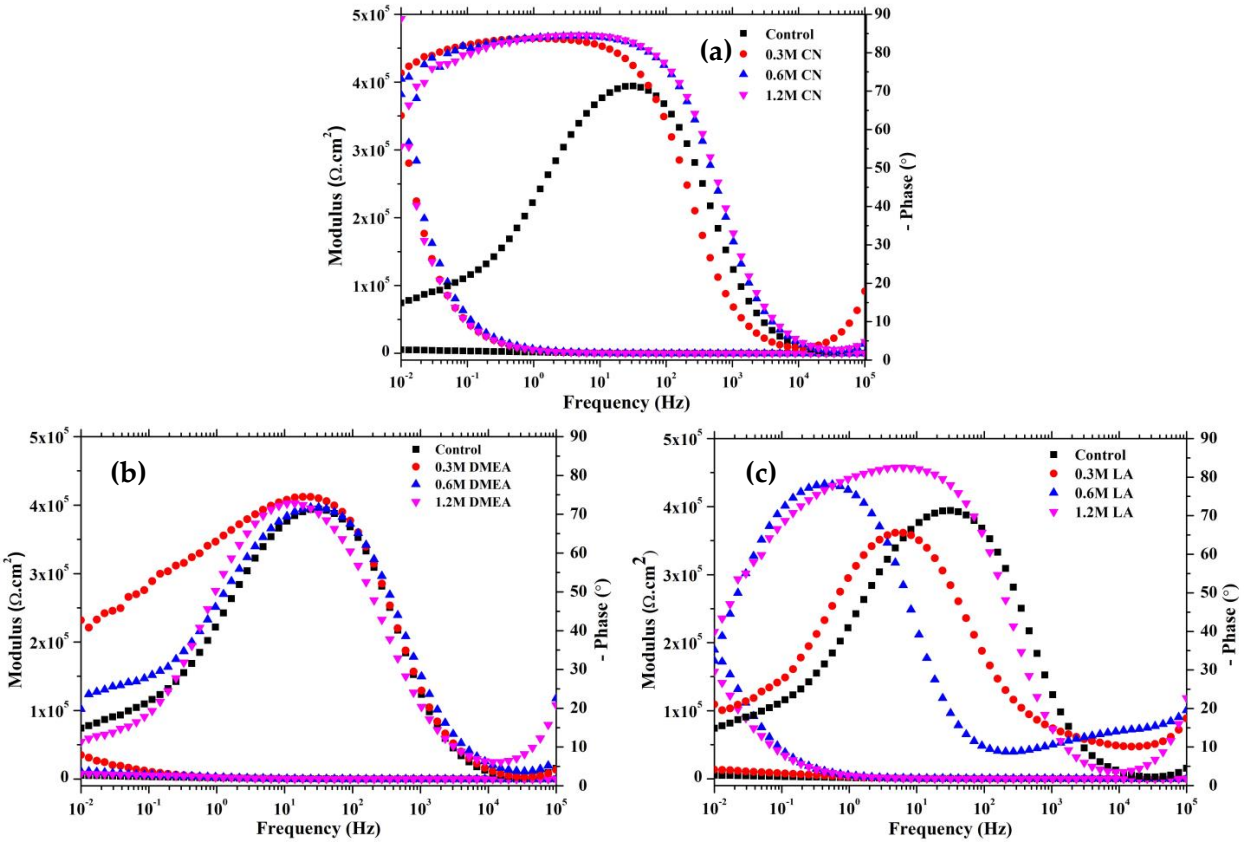

Figure 3. Modulus and phase frequency Bode plots of steel rebar immersed in NCCP solution with different concentrations of (**a**) CN, (**b**) DMEA, and (**c**) LA after 1 h.

The steel rebar was continuously immersed in solution for up to 168 h, and the EIS results are presented in Figures 4 and 5. The Nyquist plots after 168 h of immersion are shown in Figure 4. The Nyquist plots for the CN inhibitor are shown in Figure 4a. It can be observed that the CN inhibitor-containing samples show a decrease in the magnitude of the Nyquist plots for all concentrations, which is attributed to localized attack of the Cl^{-} ions present in the solution leading to perturb the oxide layer. However, the imaginary component of the Nyquist plot at lower frequencies is larger than the real component, indicating the defective oxide layer on the steel surface. The capacitive loop at low frequencies (arrow mark in Figure 4a) is more pronounced than that at high frequencies. From this plot, it can be seen that higher concentrations of CN form a strong passive film, which significantly enhances the corrosion resistance of the steel rebar immersed in the

NCCP solution; however, at extended periods of immersion, the defective oxide film starts to dissolve.

The Nyquist plots for DMEA-containing inhibitors after 168 h of immersion in the NCCP solution are shown in Figure 4b. The magnitude of the Nyquist plots of 0.3 M DMEA after 168 h is higher than that observed at 1 h, which is attributed to the adsorption of inhibitor molecules and the formation of a passive film. At lower concentrations of DMEA, the Nyquist plot magnitude is greater compared to higher concentrations. In smaller amounts of DMEA, the nitrogen atom forms a covalent bond with Fe through its lone pair of electrons. However, at higher concentrations, the methyl and ethyl groups of DMEA interfere with the nitrogen's interaction with Fe, weakening the bond. As a result, the Nyquist plot magnitude for higher concentrations of DMEA is reduced compared to lower concentrations. The low-frequency capacitive loop for lower concentrations of DMEA is larger than that at high frequencies, indicating a stronger adsorption tendency between the DMEA and Fe.

The Nyquist plots for LA-containing inhibitors after 168 h of immersion in NCCP solution are shown in Figure 4c. Interestingly, the dimensions of the Nyquist plots for the LA-containing samples remain nearly identical to those observed after 1 h, except for the 0.6 M LA sample, indicating that the film is protective. Despite a decrease in the plot magnitude for the 0.6 M LA sample, it is still greater than that of the other samples, suggesting that the formed complex is protective. However, residual Cl^- ions in the NCCP solution locally attack and weaken the bonding, leading to the destabilization of the film. The low-frequency capacitive loop of the Nyquist plot for the LA inhibitor is larger than those at middle and high frequencies, indicating that the complexes, such as zwitterion-(Cl)-Fe and zwitterion-Fe, are responsible for the observed charge transfer resistance (R_{ct}). The magnitude of the low-frequency capacitive loop is larger than that of the middle and high frequencies, as shown in Figure 4c. Additionally, the 0.6 M and 1.2 M LA inhibitor-containing samples display similar dimensions at low frequencies, indicating the adsorption of inhibitor molecules and the formation of an adherent complex.

The modulus–frequency and phase angle–frequency Bode plots of the samples after 168 h of immersion are shown in Figure 5. The total impedance values for the CN inhibitor-containing samples at 0.01 Hz decreased after 168 h of exposure (Figure 5a) compared to 1 h, indicating that the oxide layer formed after 1 h of immersion is defective, which leads to the dissolving of the film. There is a broadening of the phase angle maxima from the middle to low frequencies, around -80°, in the inhibitor-containing samples, while the control sample exhibits an asymmetric capacitive loop at middle frequencies, as shown in Figure 5a. The broadening of the phase angle maxima suggests the formation of a homogeneous oxide layer, while the asymmetric capacitive loop in the control sample indicates the development of a defective and porous oxide layer on the steel surface in presence and absence of CN inhibitor. These findings suggest that the CN inhibitor has strong oxidizing properties, protecting the steel rebar from corrosion in an aggressive concrete environment.

The total impedance of the steel rebar containing 0.3 M DMEA inhibitor gradually increased after 168 h of immersion, while higher concentrations of DMEA showed a decrease, as illustrated in Figure 5b, when compared to the results after 1 h. This increase in impedance for the 0.3 M DMEA sample is attributed to the effective adsorption of inhibitor molecules, whereas the destabilization of the adsorbed layer occurs at higher concentrations of the inhibitor. In higher amounts of DMEA, the methyl and ethyl groups, along with Cl^- ions from the NCCP solution, synergistically destabilize the adsorbed inhibitor molecules on the steel rebar, leading to film deterioration. The phase angle Bode plots in Figure 5b show that all samples exhibit two time constants at middle and low frequencies. The 0.3 M DMEA sample, however, displays broadening in the capacitive loop at middle frequencies and a shift in the low-frequency maximum to around -60°, suggesting the formation of a highly protective film. This film is physiochemically adsorbed and effectively inhibits the surface from chloride attack. The low-frequency maxima for this sample also shows a greater phase angle shift compared to the results after 1 h of immersion. In contrast, the

other samples display asymmetric capacitive loops at middle frequencies due to less stable adsorption of the inhibitor molecules.

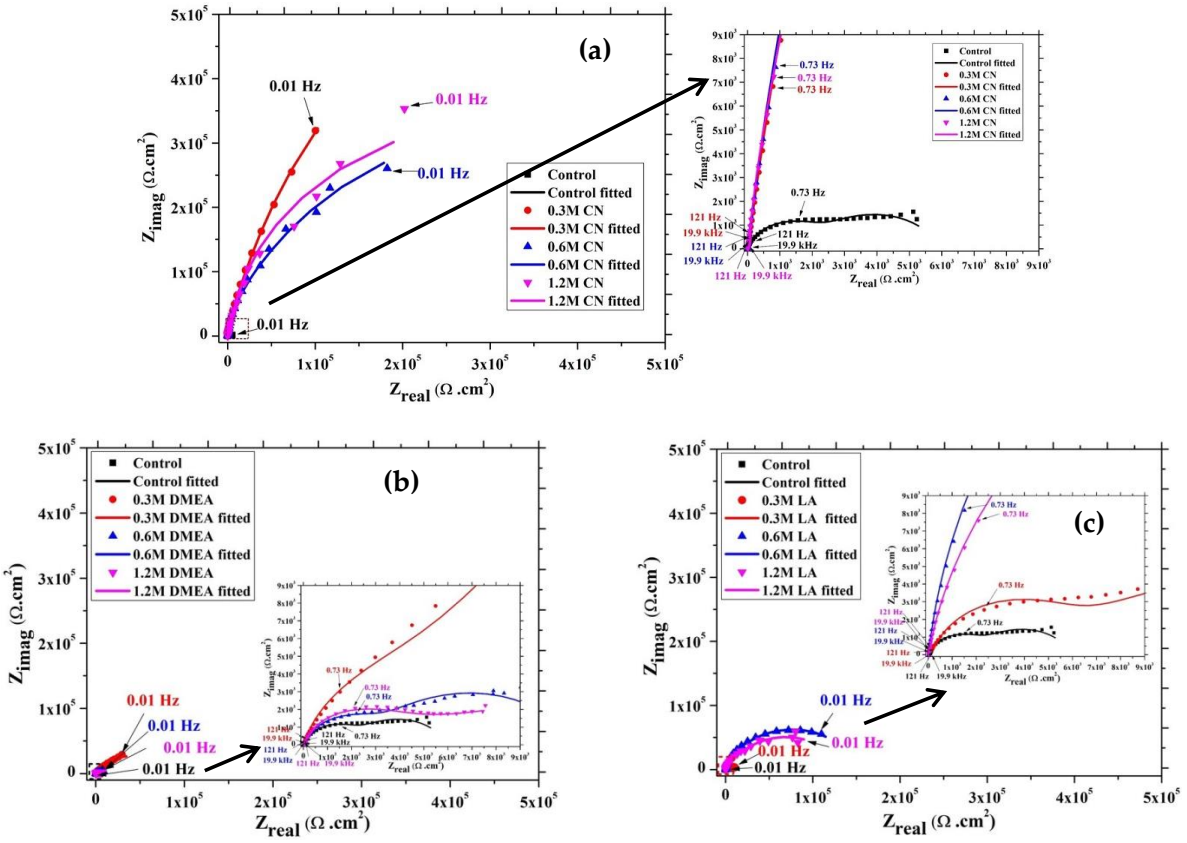

Figure 4. The Nyquist plots of steel rebar immersed in NCCP solution with different concentrations of (**a**) CN, (**b**) DMEA, and (**c**) LA after 168 h.

The total impedance of LA-containing inhibitors remains largely stable, with nearly identical impedance values observed after 1 h and 168 h of immersion, except for the 0.6 M LA sample, as shown in Figure 5c. This suggests that once LA is introduced into the NCCP solution, the pre-formed Cl-Fe complex interacts with the LA zwitterion to form a zwitterion-(Cl)-Fe complex, stabilizing the film and enhancing corrosion protection over extended exposure, unless the chloride concentration increases. Due to the small atomic radii of the Cl^- ion, it readily interacts with Fe^{++}, whereas zwitterion exhibits a greater atomic size. Thus, Cl-Fe could form first, and then after, zwitterion interacts with Cl-Fe to form the zwitterion-(Cl)-Fe complex. Although the total impedance of the 0.6 M LA sample decreases after 168 h, it still shows the highest values among all concentrations. The phase angle maxima after 168 h of immersion, shown in Figure 5c, indicates that the 0.6 M LA sample has the highest phase angle maximum and broadening from middle to low frequencies. This suggests that the adsorbed layer on the steel rebar is homogeneous and protective due to the formation of the zwitterion-(Cl)-Fe complex. In contrast, the control sample shows a phase angle maxima at high and middle frequencies, indicating a porous and unprotective oxide layer caused by Cl^- ions, which accelerates corrosion after 168 h. The 0.3 M LA sample has a lower phase angle maximum located at middle frequencies, suggesting the formation of a porous film that is still more protective than the control. Additionally, the 0.6 M and 1.2 M LA samples exhibit similar capacitive properties, but the 1.2 M LA sample has a lower phase angle maximum compared to the 0.6 M sample. This indicates that the film formed in the 1.2 M LA solution has some vacancies, leading to lower total impedance than the 0.6 M LA sample. This is attributed to the zwitterion

adsorbing through the carboxylic group rather than the NH_2 group, due to the chloride concentration being below the optimal level.

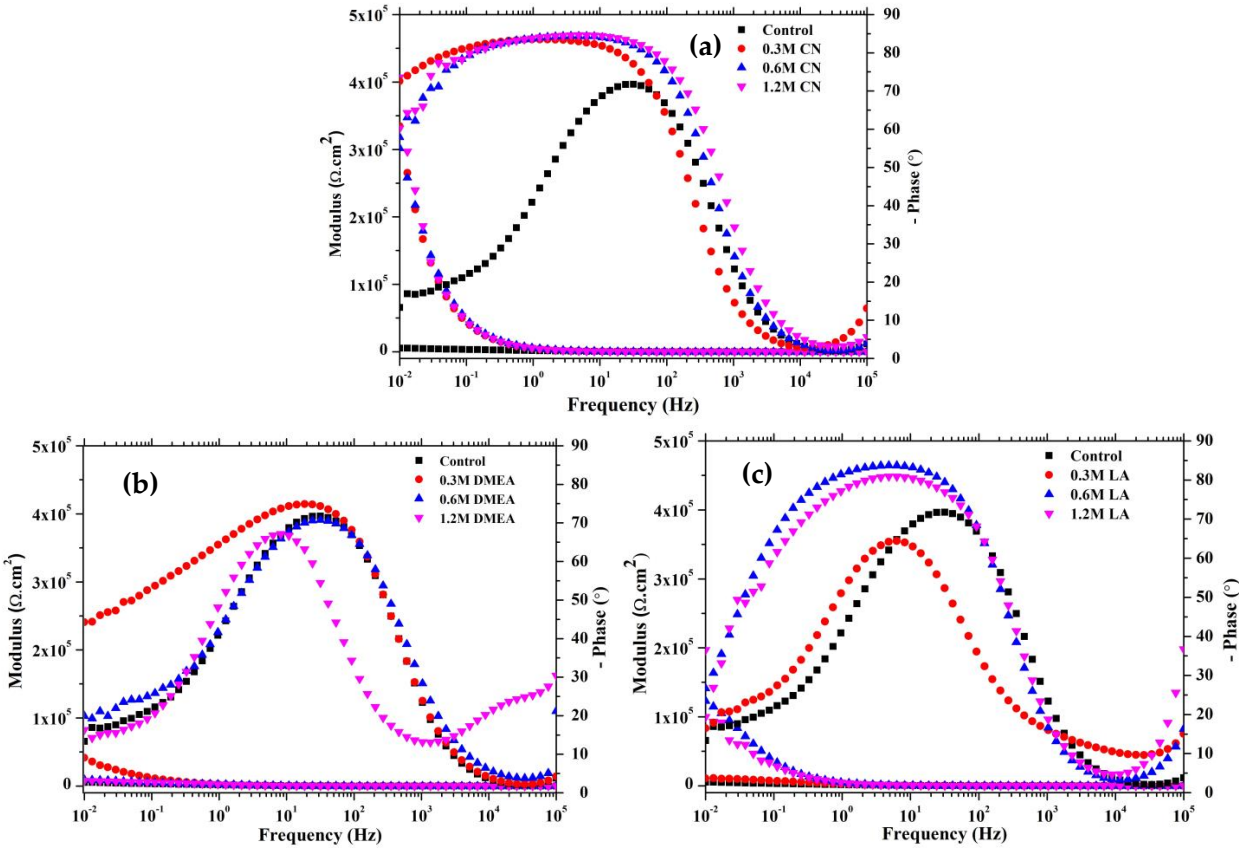

Figure 5. Modulus and phase frequency Bode plots of steel rebar immersed in NCCP solution with different concentrations of (**a**) CN, (**b**) DMEA, and (**c**) LA after 168 h.

A suitable electrical equivalent circuit (EEC) is required to fit the EIS data. In the present study, the EIS results show two time constants at middle and low frequencies. Accordingly, the appropriate EEC is presented in Figure 6 to fit the data [22,23,49,50]. In this figure, the first time constant, occurring at middle frequencies, corresponds to the oxide/passive film, while the second time constant, at low frequencies, relates to the interface between the passive/oxide film and the steel rebar. In this EEC, the first time constant is associated with the solution resistance (R_s) and a constant phase element of the film (CPE_f), which is in parallel with the film resistance (R_f). The second time constant at low frequencies involves charge transfer, represented by the constant phase element (CPE_{ct}) and charge transfer resistance (R_{ct}), which are also in parallel.

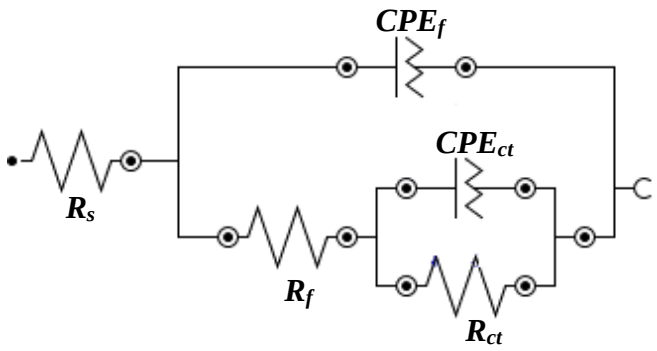

Figure 6. EEC of the samples.

The electrochemical parameters extracted from fitting the EIS plots to the appropriate EEC are presented in Table 3. The R_s values for the CN inhibitor are slightly higher compared to other inhibitors, likely due to its reduced dissolution in the NCCP solution. Notably, the R_f values for all inhibitors, except for 0.6 M LA, are higher than the R_{ct} values, indicating the adsorption of inhibitor molecules and the formation of a protective film on the steel rebar. In the case of 0.6 M LA, the R_{ct} is greater than the R_f, suggesting the formation of a highly adherent and protective film that effectively prevents electron transfer from the metal surface to the solution. The control sample exhibits the lowest R_f and R_{ct} values, indicating minimal corrosion protection in the absence of an effective inhibitor in the NCCP solution. The constant phase element (CPE) exponent values for the film (n_f) and charge transfer (n_{ct}) of the CN inhibitor are $\geq$0.8, suggesting that the film is homogeneous, which aligns with the phase–frequency Bode plots (Figures 3a and 5a), where the phase angle maxima approach $-80°$. For DMEA, the n_f and n_{ct} values are less than 0.8, indicating a heterogeneous and defective film that can initiate corrosion. However, the 0.6 M and 1.2 M LA inhibitors demonstrate the formation of a homogeneous passive/oxide film layer. The CPE component for film (Q_f) and charge transfer (Q_{ct}) values of control sample are the highest among all the samples, indicating that the oxide layer is defective and exhibits capacitive properties. Similarly, the 0.6 M and 1.2 M DMEA, as well as the 0.3 M LA samples, also show high values, which are attributed to vacancies in the film and a defective oxide layer, respectively.

Table 3. The electrochemical parameters extracted after fitting of EIS plots in suitable EEC.

Sample ID	Time	Electrochemical Parameters							IE%
		R_s ($\Omega.cm^2$)	R_f ($k\Omega.cm^2$)	CPE_f		R_{ct} ($k\Omega.cm^2$)	CPE_{ct}		
				Qf (1×10^{-5}) ($\Omega^{-1}.cm^{-2}.s^n$)	n_f		Q_{ct} (1×10^{-5}) ($\Omega^{-1}.cm^{-2}.s^n$)	n_{ct}	
Control	1 h	13.14	3.14	37.61	0.68	2.19	39.20	0.66	0
0.3 M CN		14.54	244.80	3.62	0.94	107.12	4.67	0.90	97.96
0.6 M CN		18.81	255.37	3.16	0.94	126.28	4.16	0.92	98.27
1.2 M CN		31.45	347.30	2.04	0.98	146.05	3.74	0.92	98.50
0.3 M DMEA		13.19	22.62	10.81	0.77	12.32	19.62	0.74	82.22
0.6 M DMEA		16.21	6.94	15.78	0.71	4.84	22.04	0.70	54.75
1.2 M DMEA		20.03	4.50	24.25	0.70	3.34	26.93	0.68	34.43
0.3 M LA		14.74	8.39	12.97	0.74	5.12	17.72	0.71	57.23
0.6 M LA		17.45	70.13	5.76	0.85	119.42	3.33	0.92	98.17
1.2 M LA		22.35	107.11	4.13	0.90	50.41	8.60	0.84	95.66
Control	168 h	13.02	3.20	36.02	0.69	2.15	39.49	0.66	0
0.3 M CN		14.72	232.85	4.06	0.94	101.68	4.23	0.89	97.89
0.6 M CN		18.92	220.15	4.17	0.93	98.02	4.93	0.89	97.81
1.2 M CN		31.31	282.48	3.41	0.96	124.32	4.28	0.92	98.27
0.3 M DMEA		13.92	25.20	10.49	0.78	16.41	18.39	0.75	86.90
0.6 M DMEA		16.24	6.23	16.68	0.71	3.36	25.75	0.67	36.01
1.2 M DMEA		20.24	4.61	23.52	0.70	3.28	27.10	0.68	34.45
0.3 M LA		14.44	6.57	16.37	0.71	4.19	24.36	0.69	48.69
0.6 M LA		17.90	43.90	10.84	0.82	79.22	5.33	0.88	97.29
1.2 M LA		22.32	68.79	5.96	0.85	30.91	12.27	0.78	93.04

The corrosion inhibition efficiency (IE%) of inhibitor based on R_{ct} values is calculated by [51–53]:

$$\text{IE\%} = \left(\frac{R_{ct\ (inhibitor)} - R_{ct\ (control)}}{R_{ct\ (inhibitor)}} \right) \times 100 \quad (1)$$

where $R_{ct(inhibitor)}$ and $R_{ct(control)}$ represent the charge transfer resistance of the inhibitor-containing sample and the control sample, respectively, as shown in Table 3. From the data in Table 3, it is clear that the inhibition efficiency (IE%) of the CN inhibitor remains consistently around 98% for all concentrations, even after 1 and 168 h of immersion. Similarly, 0.6 M LA exhibits a stable inhibition efficiency of 98% across all immersion durations. The 1.2 M LA inhibitor also shows an efficiency of over 90% after both 1 and 168 h of immersion. Additionally, the 0.3 M DMEA inhibitor demonstrates an inhibition efficiency greater than 80%, which qualifies it as a viable inhibitor, as other studies have suggested that a minimum IE% of 80% is required for an inhibitor to be considered effective in building materials [54]. These findings suggest that instead of using CN, which has been banned in many countries due to its hazardous nature, eco-friendly alternatives such as 0.3 M DMEA, 0.6 M LA, and 1.2 M LA can be used as effective corrosion inhibitors for steel in concrete.

3.1.3. Potentiodynamic Polarization (PDP) Studies After 168 h of Immersion

Figure 7a–c display the PDP curves of the CN-, DMEA-, and LA-containing inhibitors after 168 h of immersion in the NCCP solution. The cathodic curves of all samples show an oxygen-reduction reaction, attributed to the adsorption of inhibitor molecules or the formation of an oxide film, where oxygen is reduced within the oxide film. In Figure 7a, the 0.6 M and 1.2 M CN samples are significantly cathodically polarized, indicating the formation of a strong passive film. During the anodic scanning of the control and 0.3 M CN samples, there is a gradual increase in current from the corrosion potential (E_{corr}) at a certain OCP, after which the passive film begins to form. However, the current density of these samples is higher compared to the 0.6 M and 1.2 M CN samples. Additionally, many breakdown in OCP is observed in the 0.6 M and 1.2 M CN samples during anodic scanning, attributed to the formation of a mixed/metastable oxide film, as noted by Ryu et al. (2017) in their study on the effect of calcium nitrite inhibitors on corrosion mitigation in chloride-contaminated solutions [37]. As the concentration of CN inhibitor increases, the anodic current density decreases. However, a sharp increase in the anodic current of the 1.2 M CN sample at 0.400 V vs. SCE suggests pit formation.

The weak adsorption of the DMEA inhibitor at higher concentrations, as previously discussed, indicates that the bonding between the inhibitor and Fe (steel rebar) weakens, leading to an increase in cathodic current. As a result, samples containing 0.6 M and 1.2 M DMEA show higher cathodic current compared to the 0.3 M sample, as depicted in Figure 7b. These higher concentration samples are less polarized than the 0.3 M DMEA sample. During anodic scanning, an increase in DMEA concentration leads to a rise in current, suggesting that the protective film becomes unstable and promotes corrosion. However, when compared to the control sample, DMEA-containing samples still demonstrate better corrosion resistance. Therefore, it is recommended to use the lowest concentration of DMEA, as it shows superior performance over higher concentrations.

Figure 7c illustrates the PDP curve for steel rebar immersed in various concentrations of LA inhibitor in NCCP solution after 168 h. From the figure, it is evident that samples containing LA undergo an oxygen-reduction reaction during cathodic polarization. This finding suggests that the protective film formed on the steel rebar is reduced, leading to a weakening of the film [41]. In the case of 0.3 M LA, the film is unstable and easily degraded by Cl^- ions, resulting in a higher cathodic current density compared to other LA concentrations. During anodic scanning, the 0.6 M and 1.2 M LA samples exhibit passive film formation, where the zwitterion-(Cl)-Fe complex stabilizes and protects the steel rebar from corrosion. In contrast, for the control sample and the 0.3 M LA sample, the

current gradually increases during anodic scanning from the corrosion potential (E_{corr}), indicating film dissolution. The anodic current densities of the 0.6 M and 1.2 M LA samples are nearly identical, suggesting that the films are stable and adherent, offering effective corrosion protection.

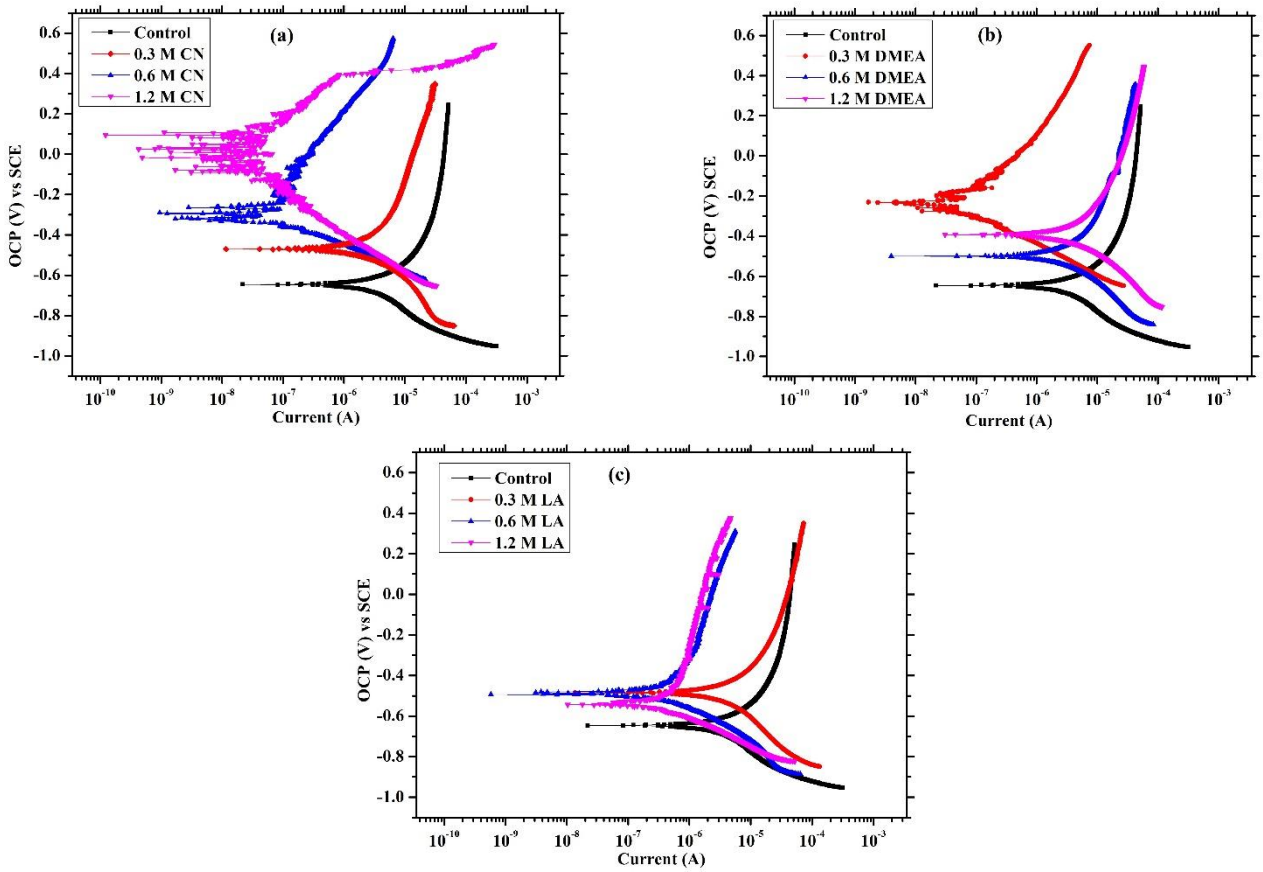

Figure 7. PDP curves of (**a**) CN, (**b**) DMEA, and (**c**) LA inhibitor containing steel rebar after 168 h of immersion in NCCP solution.

3.2. Characterization of Surface Film by SEM

Figure 8a,b present SEM images of the surface films formed on the control sample and the 0.6 M LA sample, respectively, after 168 h of immersion in the NCCP solution. The control sample lacks an inhibitor, while the 0.6 M LA solution, known for its eco-friendly properties, demonstrates excellent corrosion resistance. As a result, only these two solutions were selected for SEM analysis of the surface film morphology. In Figure 8a, the control sample shows a defective film with localized attacks by Cl^- ions from the NCCP solution, leading to pit formation [36]. This results in the lowest corrosion resistance among all samples as observed in EIS and PDP analysis. Conversely, the 0.6 M LA sample forms a uniform and adherent film, as shown in Figure 8b. This is attributed to the formation of a zwitterion-(Cl)-Fe complex, which provides effective corrosion protection. The scratches visible on both samples are due to polishing, as fine, unavoidable scratches remain.

The surface film's chemical composition, characterized using EDS, is presented in Table 4. These data show that the control sample has a high oxygen (O) content, suggesting the formation of oxide or corrosion products on the steel rebar surface as a result of corrosion. Elements like Na, K, Ca, and Cl are also present, originating from the NCCP solution composition. In contrast, the 0.6 M LA sample displays the presence of C and N, indicating the adsorption of the zwitterion ($C_6H_{14}N_4O_2$) and the formation of a zwitterion-(Cl)-Fe complex on the rebar surface. The control sample's elevated Cl content further promotes corrosion, which is observed on the surface. However, in the 0.6 M LA sample,

only a minimal amount of Cl is detected, suggesting that most Cl^- ions were consumed in forming the zwitterion-(Cl)-Fe complex.

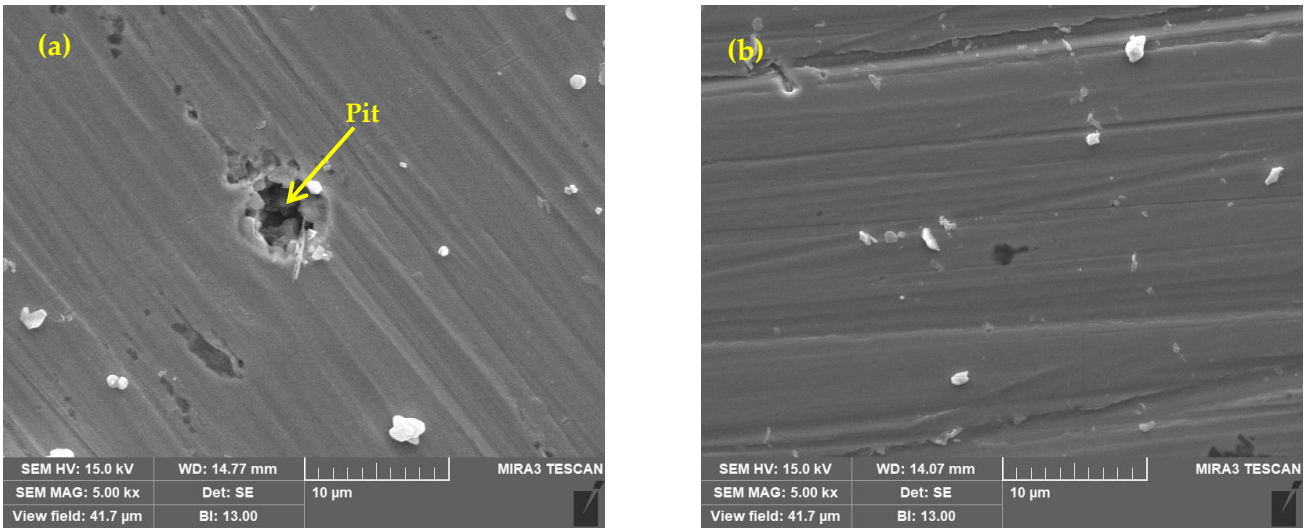

Figure 8. The surface morphology of the steel rebar at 5000× magnification after 168 h of immersion in (**a**) the control (NCCP) and (**b**) the 0.6 M LA solution containing NCCP solution.

Table 4. EDS analysis of the surface film.

Sample ID	Elements (wt.%)							
	C	N	O	Na	Cl	Ca	K	Fe
Control	0.11	-	12.95	1.56	2.38	0.78	0.35	81.87
0.6 M LA	12.09	5.31	2.55	1.17	0.21	0.89	0.38	77.40

4. Conclusions

Steel rebar samples were immersed in a NCCP solution with different inhibitors—CN, DMEA, and LA—and their corrosion performances were assessed over varying concentrations and immersion durations. The following conclusions have been drawn from the present studies:

(a) The OCP of the control sample shifted in the active direction up to 72 h, after which it stabilized, likely due to the formation of corrosion products. Samples containing the CN inhibitor shifted their OCP in the positive direction, except for the 0.3 M concentration, likely due to the oxidation of Fe^{2+} to Fe^{3+}. Conversely, samples with the DMEA inhibitor showed an OCP shift in the active direction over the immersion period, except for the 0.3 M concentration, which destabilized the protective film by forming a carbonate layer. At higher concentrations of DMEA, the adsorption of methyl and ethyl groups hindered nitrogen interactions with the steel surface, while Cl^- ions accelerated corrosion. In contrast, the OCP of the 0.6 M LA sample remained stable throughout immersion, likely due to the formation of a zwitterion-(Cl)-Fe complex.

(b) OCP results show that the 1.2 M CN inhibitor shifted the OCP beyond the corrosion initiation zone, with 0.6 M LA proving to be even more effective. LA concentrations lower or higher than 0.6 M shifted the OCP toward more active regions. In contrast, DMEA-containing samples displayed active OCP values, remaining within the corrosion initiation zone. This suggests that a higher concentration of CN is required to establish a protective passive or oxide film, while 0.6 M LA maintains a stable passive state in the NCCP solution.

(c) The total impedance of samples containing the CN inhibitor gradually decreased over the immersion period, suggesting a defective oxide film on the steel rebar, destabilized by Cl^- ions. In contrast, the 0.3 M DMEA sample showed an increase in impedance due to the adsorption of inhibitor molecules, while other concentrations resulted in decreased impedance. Meanwhile, samples with the LA inhibitor maintained stable impedance throughout the immersion period, likely due to the formation of a zwitterion-(Cl)-Fe complex.

(d) EIS results show that all samples exhibited higher R_f values compared to R_{ct}, except for the 0.6 M LA sample, indicating the adsorption of inhibitor molecules and the formation of a protective film on the steel rebar. For the 0.6 M LA sample, however, the R_{ct} value is greater than the R_f, suggesting that it effectively inhibits the electron transfer from the metal surface to the solution.

(e) Both 0.6 M and 1.2 M CN exhibited corrosion resistance efficiencies greater than 98%, maintaining this performance over time. Similarly, 0.6 M LA showed identical corrosion inhibition efficiency, indicating that LA, being eco-friendly and effective, could be a better alternative to CN.

(f) The optimal concentrations of each inhibitor—1.2 M CN, 0.3 M DMEA, and 0.6 M LA—showed multiple OCP breakdowns during anodic scanning, likely due to the formation of a mixed or metastable oxide film. This behavior indicates their excellent performance.

(g) SEM of the control sample revealed pitting due to localized chloride attack, while the steel rebar immersed in 0.6 M LA-containing NCCP solution exhibited a uniform and adherent film, resulting in enhanced corrosion resistance.

(h) It is suggested that the corrosion resistance performance of DMEA and LA inhibitors be evaluated in real concrete, offering a new direction for the application of eco-friendly corrosion inhibitors in concrete.

Author Contributions: Conceptualization, H.-S.L. and J.K.S.; funding acquisition, H.-S.L.; investigation, S.-H.M., H.-S.L. and J.K.S.; methodology, S.-H.M. and J.K.S.; writing—original draft, S.-H.M., H.-S.L. and J.K.S.; writing—review, S.-H.M., H.-S.L. and J.K.S. All authors have read and agreed to the published version of the manuscript.

Funding: This work was supported by the National Research Foundation of Korea (NRF) grant funded by the Korea government (No. NRF-2018R1A5A1025137).

Data Availability Statement: Data are contained within the article.

Conflicts of Interest: The authors declare no conflicts of interest.

References

1. Valcarce, M.B.; Vázquez, M. Carbon steel passivity examined in alkaline solutions: The effect of chloride and nitrite ions. *Electrochim. Acta* **2008**, *53*, 5007–5015. [CrossRef]
2. Pokorný, P.; Kostelecka, M.; Prodanovic, N.; Sýkora, M. Effect of calcium hydroxyzincate on bond strength of hot-dip galvanized plain bars with normal strength concrete. *Cem. Concr. Compos.* **2022**, *130*, 104540. [CrossRef]
3. Pokorný, P.; Chobotský, T.; Prodanovic, N.; Steinerová, V.; Hurtig, K. Bond Strength and Corrosion Protection Properties of Hot-Dip Galvanized Prestressing Reinforcement in Normal-Strength Concrete. *J. Compos. Sci.* **2024**, *8*, 407. [CrossRef]
4. Hamad, B.S.; Mike, J.A. Bond strength of hot-dip galvanized reinforcement in normal strength concrete structures. *Constr. Build. Mater.* **2005**, *19*, 275–283. [CrossRef]
5. Pokorný, P.; Pernicová, R.; Tej, P.; Kolísko, J. Changes of bond strength properties of hot-dip galvanized plain bars with cement paste after 1 year of curing. *Constr. Build. Mater.* **2019**, *226*, 920–931. [CrossRef]
6. Singh, D.D.N.; Ghosh, R. Unexpected deterioration of fusion-bonded epoxy-coated rebars embedded in chloride-contaminated concrete environments. *Corrosion* **2005**, *61*, 815–829. [CrossRef]
7. Umoren, S.A. Biomaterials for corrosion protection: Evaluation of mustard seed extract as eco-friendly corrosion inhibitor for X60 steel in acid media. *J. Adhes. Sci. Technol.* **2016**, *30*, 1858–1879. [CrossRef]
8. Tansug, G. Synergistic inhibition effect between 4-amino-5-methyl-4H-1, 2, 4-triazole-3-thiol, citrate ions and polycarboxylate for corrosion protection of C1010 steel in cooling water system. *J. Adhes. Sci. Technol.* **2017**, *31*, 2053–2070. [CrossRef]
9. Menaka, R.; Subhashini, S. Chitosan Schiff base as eco-friendly inhibitor for mild steel corrosion in 1 M HCl. *J. Adhes. Sci. Technol.* **2016**, *30*, 1622–1640. [CrossRef]

10. El-Haddad, M.A.; Bahgat Radwan, A.; Sliem, M.H.; Hassan, W.M.; Abdullah, A.M. Highly efficient eco-friendly corrosion inhibitor for mild steel in 5 M HCl at elevated temperatures: Experimental & molecular dynamics study. *Sci. Rep.* **2019**, *9*, 3695.
11. Raja, P.B.; Ismail, M.; Ghoreishiamiri, S.; Mirza, J.; Ismail, M.C.; Kakooei, S.; Rahim, A.A. Reviews on corrosion inhibitors: A short view. *Chem. Eng. Commun.* **2016**, *203*, 1145–1156. [CrossRef]
12. Tran, D.T.; Lee, H.-S.; Singh, J.K. Chloride threshold determination of hybrid inhibitor immersed in simulated concrete pore solution. *Constr. Build. Mater.* **2023**, *384*, 131446. [CrossRef]
13. Ngala, V.; Page, C.L.; Page, M. Corrosion inhibitor systems for remedial treatment of reinforced concrete. Part 1: Calcium nitrite. *Corros. Sci.* **2002**, *44*, 2073–2087. [CrossRef]
14. Medford, W.M. Testing calcium nitrite corrosion inhibitor in concrete. *Transp. Res. Rec. J. Transp. Res. Board* **2002**, *1795*, 62–65. [CrossRef]
15. Ormellese, M.; Berra, M.; Bolzoni, F.; Pastore, T. Corrosion inhibitors for chlorides induced corrosion in reinforced concrete structures. *Cem. Concr. Res.* **2006**, *36*, 536–547. [CrossRef]
16. Reou, J.; Ann, K. The electrochemical assessment of corrosion inhibition effect of calcium nitrite in blended concretes. *Mater. Chem. Phys.* **2008**, *109*, 526–533. [CrossRef]
17. Garcés, P.; Saura, P.; Méndez, A.; Zornoza, E.; Andrade, C. Effect of nitrite in corrosion of reinforcing steel in neutral and acid solutions simulating the electrolytic environments of micropores of concrete in the propagation period. *Corros. Sci.* **2008**, *50*, 498–509. [CrossRef]
18. Ma, I.W.; Ammar, S.; Kumar, S.S.; Ramesh, K.; Ramesh, S. A concise review on corrosion inhibitors: Types, mechanisms and electrochemical evaluation studies. *J. Coat. Technol. Res.* **2022**, *19*, 241–268. [CrossRef]
19. Lee, H.-S.; Yang, H.-M.; Singh, J.K.; Prasad, S.K.; Yoo, B. Corrosion mitigation of steel rebars in chloride contaminated concrete pore solution using inhibitor: An electrochemical investigation. *Constr. Build. Mater.* **2018**, *173*, 443–451. [CrossRef]
20. Mandal, S.; Singh, J.K.; Lee, D.-E.; Park, T. Ammonium phosphate as inhibitor to mitigate the corrosion of steel rebar in chloride contaminated concrete pore solution. *Molecules* **2020**, *25*, 3785. [CrossRef]
21. Mandal, S.; Singh, J.K.; Lee, D.-E.; Park, T. Effect of Phosphate-Based Inhibitor on Corrosion Kinetics and Mechanism for Formation of Passive Film onto the Steel Rebar in Chloride-Containing Pore Solution. *Materials* **2020**, *13*, 3642. [CrossRef]
22. Yohai, L.; Schreiner, W.; Valcarce, M.; Vázquez, M. Inhibiting steel corrosion in simulated concrete with low phosphate to chloride ratios. *J. Electrochem. Soc.* **2016**, *163*, C729. [CrossRef]
23. Yohai, L.; Vázquez, M.; Valcarce, M. Phosphate ions as corrosion inhibitors for reinforcement steel in chloride-rich environments. *Electrochim. Acta* **2013**, *102*, 88–96. [CrossRef]
24. Ormellese, M.; Lazzari, L.; Goidanich, S.; Fumagalli, G.; Brenna, A. A study of organic substances as inhibitors for chloride-induced corrosion in concrete. *Corros. Sci.* **2009**, *51*, 2959–2968. [CrossRef]
25. Li, Y.; Zhang, Y.; Jungwirth, S.; Seely, N.; Fang, Y.; Shi, X. Corrosion inhibitors for metals in maintenance equipment: Introduction and recent developments. *Corros. Rev.* **2014**, *32*, 163–181. [CrossRef]
26. Elshami, A.; Bonnet, S.; Khelidj, A.; Sail, L. Effectiveness of corrosion inhibitors in simulated concrete pore solution. *Eur. J. Environ. Civ. Eng.* **2020**, *24*, 2130–2150. [CrossRef]
27. Lee, H.-S.; Ryu, H.-S.; Park, W.-J.; Ismail, M.A. Comparative study on corrosion protection of reinforcing steel by using amino alcohol and lithium nitrite inhibitors. *Materials* **2015**, *8*, 251–269. [CrossRef]
28. Raffaini, G.; Catauro, M.; Ganazzoli, F.; Bolzoni, F.; Ormellese, M. Organic Inhibitors to Prevent Chloride-Induced Corrosion in Concrete: Atomistic Simulations of Triethylenetetramine-Based Inhibitor Film. *Macromol. Symp.* **2021**, *395*, 2000231. [CrossRef]
29. Rakanta, E.; Zafeiropoulou, T.; Batis, G. Corrosion protection of steel with DMEA-based organic inhibitor. *Constr. Build. Mater.* **2013**, *44*, 507–513. [CrossRef]
30. Ryu, H.-S.; Singh, J.K.; Yang, H.-M.; Lee, H.-S.; Ismail, M.A. Evaluation of corrosion resistance properties of N, N′-Dimethyl ethanolamine corrosion inhibitor in saturated $Ca(OH)_2$ solution with different concentrations of chloride ions by electrochemical experiments. *Constr. Build. Mater.* **2016**, *114*, 223–231. [CrossRef]
31. Ryu, H.-S.; Singh, J.K.; Lee, H.-S.; Ismail, M.A.; Park, W.-J. Effect of LiNO2 inhibitor on corrosion characteristics of steel rebar in saturated Ca (OH) 2 solution containing NaCl: An electrochemical study. *Constr. Build. Mater.* **2017**, *133*, 387–396. [CrossRef]
32. Fouda, A.S.; Elewady, G.Y.; Shalabi, K.; El-Aziz, H.K.A. Alcamines as corrosion inhibitors for reinforced steel and their effect on cement based materials and mortar performance. *RSC Adv.* **2015**, *5*, 36957–36968. [CrossRef]
33. Singh, D.; Ghosh, R. Corrosion resistance performance of fusion bonded epoxy coated rebars used as reinforcement in concrete structures. *J. Metall. Mater. Sci.* **2003**, *45*, 73–83.
34. Ghosh, R.; Singh, D. Kinetics, mechanism and characterisation of passive film formed on hot dip galvanized coating exposed in simulated concrete pore solution. *Surf. Coat. Technol.* **2007**, *201*, 7346–7359. [CrossRef]
35. Etteyeb, N.; Dhouibi, L.; Sanchez, M.; Alonso, C.; Andrade, C.; Triki, E. Electrochemical study of corrosion inhibition of steel reinforcement in alkaline solutions containing phosphates based components. *J. Mater. Sci.* **2007**, *42*, 4721–4730. [CrossRef]
36. Tran, D.T.; Lee, H.-S.; Singh, J.K. Influence of phosphate ions on passive film formation in amino acid-containing concrete pore solutions with chloride ions. *J. Build. Eng.* **2023**, *66*, 105834. [CrossRef]
37. Ryu, H.-S.; Singh, J.K.; Lee, H.-S.; Park, W.-J. An electrochemical study to evaluate the effect of calcium nitrite inhibitor to mitigate the corrosion of reinforcement in sodium chloride contaminated $Ca(OH)_2$ solution. *Adv. Mater. Sci. Eng.* **2017**, *2017*, 6265184. [CrossRef]

38. Söylev, T.A.; McNally, C.; Richardson, M. Effectiveness of amino alcohol-based surface-applied corrosion inhibitors in chloride-contaminated concrete. *Cem. Concr. Res.* **2007**, *37*, 972–977. [CrossRef]
39. Jamil, H.E.; Montemor, M.; Boulif, R.; Shriri, A.; Ferreira, M. An electrochemical and analytical approach to the inhibition mechanism of an amino-alcohol-based corrosion inhibitor for reinforced concrete. *Electrochim. Acta* **2003**, *48*, 3509–3518. [CrossRef]
40. Singh, J.K.; Yang, H.-M.; Lee, H.-S.; Mandal, S.; Aslam, F.; Alyousef, R. Role of L-arginine on the formation and breakdown of passive film onto the steel rebars surface in chloride contaminated concrete pore solution. *J. Mol. Liq.* **2021**, *337*, 116454. [CrossRef]
41. Singh, J.K.; Mandal, S.; Lee, H.-S.; Yang, H.-M. Effect of Chloride Ions Concentrations to Breakdown the Passive Film on Rebar Surface Exposed to L-Arginine Containing Pore Solution. *Materials* **2021**, *14*, 5693. [CrossRef]
42. Badawy, W.A.; Ismail, K.M.; Fathi, A.M. Corrosion control of Cu–Ni alloys in neutral chloride solutions by amino acids. *Electrochim. Acta* **2006**, *51*, 4182–4189. [CrossRef]
43. *ASTM C876*; Standard Test Method for Corrosion Potentials of Uncoated Reinforcing Steel in Concrete. ASTM International: West Conshohocken, PA, USA, 2015.
44. Das, J.K.; Pradhan, B. Study on influence of nitrite and phosphate based inhibiting admixtures on chloride interaction, rebar corrosion, and microstructure of concrete subjected to different chloride exposures. *J. Build. Eng.* **2022**, *50*, 104192. [CrossRef]
45. Saraswathy, V.; Song, H.-W. Improving the durability of concrete by using inhibitors. *Build. Environ.* **2007**, *42*, 464–472. [CrossRef]
46. Gaidis, J.M. Chemistry of corrosion inhibitors. *Cem. Concr. Compos.* **2004**, *26*, 181–189. [CrossRef]
47. Welle, A.; Liao, J.; Kaiser, K.; Grunze, M.; Mäder, U.; Blank, N. Interactions of N, N′-dimethylaminoethanol with steel surfaces in alkaline and chlorine containing solutions. *Appl. Surf. Sci.* **1997**, *119*, 185–198. [CrossRef]
48. Sanyal, B. Organic compounds as corrosion inhibitors in different environments—A review. *Prog. Org. Coat.* **1981**, *9*, 165–236. [CrossRef]
49. Shi, J.-J.; Sun, W. Electrochemical and analytical characterization of three corrosion inhibitors of steel in simulated concrete pore solutions. *Int. J. Miner. Metall. Mater.* **2012**, *19*, 38–47. [CrossRef]
50. Monticelli, C.; Frignani, A.; Balbo, A.; Zucchi, F. Influence of two specific inhibitors on steel corrosion in a synthetic solution simulating a carbonated concrete with chlorides. *Mater. Corros.* **2011**, *62*, 178–186. [CrossRef]
51. Radwan, A.B.; Sliem, M.H.; Yusuf, N.S.; Alnuaimi, N.A.; Abdullah, A.M. Enhancing the corrosion resistance of reinforcing steel under aggressive operational conditions using behentrimonium chloride. *Sci. Rep.* **2019**, *9*, 18115. [CrossRef]
52. Mobin, M.; Zehra, S.; Parveen, M. L-Cysteine as corrosion inhibitor for mild steel in 1 M HCl and synergistic effect of anionic, cationic and non-ionic surfactants. *J. Mol. Liq.* **2016**, *216*, 598–607. [CrossRef]
53. Samide, A.; Dobrițescu, A.; Tigae, C.; Spînu, C.I.; Oprea, B. Experimental and computational study on inhibitory effect and adsorption properties of n-acetylcysteine amino acid in acid environment. *Molecules* **2023**, *28*, 6799. [CrossRef] [PubMed]
54. Yang, H.-M.; Singh, J.K.; Jang, H.-O. Ginger powder as sustainable and eco-friendly corrosion inhibitor for the protection of steel reinforcement bars. *Case Stud. Constr. Mater.* **2024**, *21*, e03821. [CrossRef]